Myeong Hee Moon

Department of Chemistry, Yonsei University, Seoul, Korea

Received June 11, 2010
Revised August 17, 2010
Accepted August 18, 2010

Review Article

Flow field-flow fractionation and multiangle light scattering for ultrahigh molecular weight sodium hyaluronate characterization

This review describes the utility of flow field-flow fractionation coupled with multiangle light scattering and differential refractive index (FlFFF-MALS-DRI) detection methods for the separation of ultrahigh molecular weight sodium hyaluronate (NaHA) materials and for the characterization of molecular weight distribution as well as structural determination. The sodium salt of hyaluronic acid (HA), NaHA, is a water-soluble polysaccharide with a broad range of molecular weights (10^5–10^8) found in various naturally occurring fluids and tissues. Basic principles of FlFFF-MALS using field programming for the separation of the degraded products of NaHA prepared by treating raw materials with depolymerization or degradation processes such as membrane filtration, enzymatic degradation, ultrasonic degradation, alkaline reaction, irradiation by γ-rays, and thermal treatment for the development of pharmaceutical applications are introduced. Changes in molecular weight distribution and conformation of NaHA materials due to external stimuli are also discussed.

Keywords: Flow field-flow fractionation / Multiangle light scattering / Sodium hyaluronate / Molecular weight distribution / Structure analysis
DOI 10.1002/jssc.201000414

1 Introduction

Sodium hyaluronate (NaHA), a sodium salt of hyaluronic acid (HA) or hyaluronan, is an ultrahigh molecular weight (MW) (10^5–10^8 in Da) water-soluble polysaccharide composed of repeating disaccharide units, D-glucuronic acid and *N*-acetyl-D-glucosamine, linked by β(1–4)-glycosidic bonds [1–3]. Hyaluronic acid is found naturally in various body fluids and tissues such as skin, synovial fluid, umbilical cord, vitreous humor, human cartilage, and rooster comb, and it plays important roles in both mechanical and transport systems in the body including lubrication of joints, regulation of molecular permeation into tissues, wound healing, control of inflammation, and other functions [1–4]. Owing to its biological safety and rheological characteristics, solutions of intact or degraded forms of NaHA have versatile uses in ophthalmic surgery as a substitute for vitreous humor, in arthritis treatment using relatively high MW molecules ($>1\times10^6$), and in wound repair and cosmetological applications with lower MW species ($<1\times10^6$) [2, 5–9]. In addition, since NaHA can absorb large amounts of water, it can be utilized as a skin moisturizer and in hydrogel formation [5–8]. Furthermore, it also aids in the spatial arrangement of tissue due to its visco-elastic properties [8]. Since the biological or pharmaceutical applications of NaHA are related to the molecular size and structure in aqueous solution, raw NaHA materials need to be processed; NaHA chains can be readily converted into smaller MW species *via* physical or chemical methods.

The molecular structure of NaHA has been reported to form a worm-like coil in dilute solution [1, 10] and a multiple helical structure stabilized by intra-chain hydrogen bonds both in the solid state [11] and in sodium chloride solution [4], according to low-angle X-ray and viscometric analysis mostly with small NaHA molecules. The molecular size of NaHA is not easy to measure by currently available methods since naturally occurring NaHA materials have a broad MWD in the ultrahigh MW regime. Analysis of the MW of NaHA materials has been studied using size exclusion chromatography (SEC) coupled with viscometric measurements [4, 12, 13], low-angle light scattering (LALS) [14], and MALDI-MS [2]. However, it is difficult to fractionate polydispersed NaHA material with an MW above a few million Daltons due to the exclusion limit of the gel matrix used in SEC. Moreover, migration of such large molecules through gels may cause shear-induced deformation of NaHA molecules or sample adsorption at the surface

Correspondence: Professor Myeong Hee Moon, Department of Chemistry, Yonsei University, Seoul 120-749, Korea
E-mail: mhmoon@yonsei.ac.kr
Fax: +82-2-364-7050

Abbreviations: DRI, differential refractive index; **FIFFF,** flow field-flow fractionation; **LALS,** low-angle light scattering; **MALS,** multiangle light scattering; **Mw,** molecular weight; **RMS,** root-mean-square; **SEC,** size exclusion chromatography

of the packing material. Lack of appropriate calibration standards is another difficulty.

In this review, the use of on-line flow field-flow fractionation (FlFFF) coupled with multiangle light scattering (MALS) and differential refractive index (DRI) methods (FlFFF-MALS-DRI) for the size separation and simultaneous determination of MWD, radius of gyration, and structural information is described. FlFFF is an elution method that fractionates macromolecules according to their hydrodynamic diameters and is utilized for the size determination or semi-preparative isolation of macromolecular species such as particles, proteins, cells, and water-soluble natural or synthetic polymers [15–20]. Since FlFFF is performed in a thin, unobstructed channel space, it is a powerful, alternative separation technique for high molecular weight polymers, especially ultrahigh MW NaHA materials, which circumvents the above-mentioned potential problems associated with SEC. On-line coupling of FlFFF with MALS has become popular for the fractionation and characterization of water-soluble polymers, especially asymmetrical FlFFF (AFIFFF) [21–24], in which a focusing/relaxation procedure is necessarily included. For the separation of ultrahigh MW NaHA materials, a frit inlet AFlFFF (FI-AFlFFF) channel system [25–27], which adopts a hydrodynamic relaxation without focusing method, has been utilized throughout these studies. This review discusses the use of AFlFFF for the MW characterization and structural determination of various NaHA materials produced by treating raw materials with various physical or chemical degradation processes such as membrane filtration, enzymatic treatment, ultrasonic degradation, irradiation by γ-rays, and thermal treatment for the development of pharmaceutical applications.

2 Principles and methods

2.1 FI-AFlFFF

FlFFF separation is carried out in an unobstructed empty channel space, which typically has a rectangular cross section *via* the use of two orthogonal flow streams: a migration flow that is directed along the channel axis toward a detector and a crossflow which moves across the channel cross section perpendicular to the migration flow. The crossflow acts as an external force to drive sample components toward one wall of the channel and, simultaneously, sample materials travel to equilibrium positions above the channel wall due to the balance of the driving force and the diffusion acting against the wall. Because smaller components exhibit faster diffusion rates than do larger components, they situate at positions further from the channel wall and elute earlier when a migration flow with a parabolic flow velocity profile is applied. Thus, separation of macromolecules by FlFFF is accomplished in the order of increasing hydrodynamic diameter (or molecular weight in some cases). In practice, the retention of molecules in FlFFF is dependent on the ratio of the crossflow and migration flow rates.

The FI-AFlFFF [25–27] channel utilized for the separation of NaHA materials is suitable for handling ultrahigh MW polymers since sample materials are injected into the channel while a relatively high-speed frit flow (usually ca. 20 times faster than the sample injection flow) is delivered to the channel through the inlet frit located at the end of the channel inlet (see Fig. 1). The role of the frit flow is to compress incoming sample components toward the channel wall so that hydrodynamic relaxation is achieved in dynamic mode without stopping the migration flow, this latter process being commonly required in conventional FlFFF. Therefore, sample relaxation and migration are continuously achieved in a facile process. FI-AFlFFF can adopt field programming by gradually reducing the crossflow rate while the crossflow circulates into the frit flow. Since the use of field programming in FlFFF can be utilized to hasten the elution of ultrahigh MW molecules with long retention times, this method has added flexibility to the processing of samples with a broad MW range. There are two different flows (sample flow and frit flow) entering the FI-AFlFFF channel and exiting as outflow and crossflow. Since field programming is often carried out with a circulation of crossflow and frit flow in FI-AFlFFF, the outflow rate is adjusted during field programming to be the same as the sample injection flow rate

$$\dot{V}_s = \dot{V}_o \text{ and } \dot{V}_f = \dot{V}_c, \quad (1)$$

where $\dot{V}$ represents the volumetric flow rate and the subscripts s, o, f, and c stand for sample flow, outflow, frit flow, and cross flow, respectively. For the programmed decay of cross flow rate, the cross flow rate at time t, $\dot{V}_c(t)$,

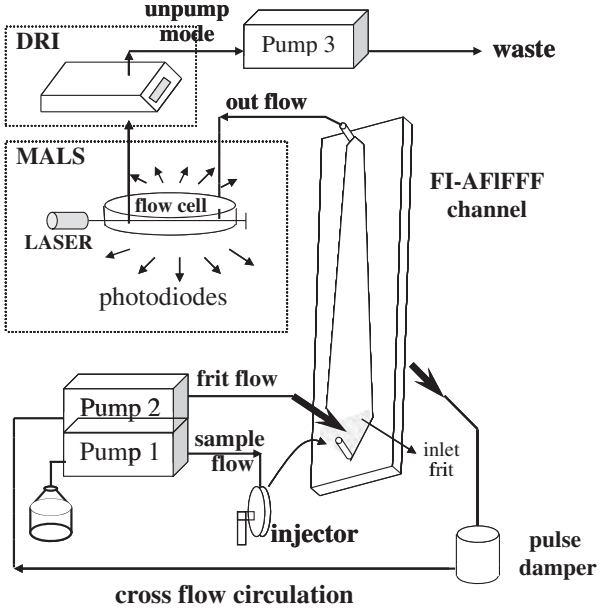

Figure 1. System configuration of FlFFF-MALS-DRI for programmed field operation with crossflow circulation.

can be simply expressed depending on the decay patterns (linear or power decay) [19] as

$$\dot{V}_c(t) = \dot{V}_{c0} - \Delta\dot{V}_c\left(\frac{t-t_1}{t_t}\right) \quad \text{for a linear decay} \tag{2}$$

$$\dot{V}_c(t) = \dot{V}_{c0}\left(\frac{t_1-t_a}{t-t_a}\right)^p \quad \text{for a power decay} \tag{3}$$

where the subscript 0 for the cross flow rate represents the initial condition before decay, $\Delta\dot{V}_c$ is the decrease in cross flow rate during the program, t_1 is the initial time delay, t_t is the transient time during decay, t_a is a time parameter ($t_a = -pt_1$), and p is a power value set to 2, known to provide a uniform fractionating power in flow FFF.

The FI-AFlFFF channel used in this study was constructed in our laboratory [25, 26] and has the channel dimensions: 27.2 cm (tip-to-tip length) × 178 μm (thickness) × 2.0 cm for the initial breadth, linearly decreasing to 1.0 cm at the final breadth (trapezoidal design). The carrier solution for FI-AFlFFF runs is 0.1 M $NaNO_3$, with 0.02% NaN_3 added as a bactericide.

2.2 Multiangle light scattering

FlFFF is on-line coupled to multiangle light scattering, size fractionation and the simultaneous determination of molecular structure as well as molecular weight according to the following relationship of light scattering intensity, R_θ, and solute concentration, c, with molecular weight, M, given as [28]

$$\frac{Kc}{R_\theta} = \frac{1}{M} + 2A_2c \quad \left(K = \frac{4\pi^2\bar{n}_0^2(dn/dc)^2}{\lambda_0^4 N_A}\right) \tag{4}$$

where A_2 is the second virial coefficient and K is a scattering constant in which λ_0 is the wavelength of incident light, $\bar{n}_0$ is the refractive index of the solvent, dn/dc is the refractive index increment with concentration, and N_A is Avogadro's number. For the case of high molecular weight polymers, Eq. (4) requires a special form factor at the observed angle, $P(\theta)$, to compensate for the phase difference caused by light scattering from different parts of the particles or from large polymers such that the equation is modified to

$$\frac{Kc}{R_\theta} = \frac{1}{P(\theta)} \times \left[\frac{1}{M} + 2A_2c\right] \quad \left(P(\theta) = 1 + \frac{16\pi^2\langle r_G^2\rangle}{3\lambda_0^2}\sin^2\left(\frac{\theta}{2}\right)\right) \tag{5}$$

where $\langle r_G^2\rangle$ is the mean-square radius of a molecule in solution. Equation (5) is utilized to calculate the molecular weight and root-mean-square (RMS) radius from the extrapolation and slope of the plot of light scattering intensity *versus* $\sin^2(\theta/2)$, respectively. Moreover, from the RMS radius (root-mean-square radius or radius of gyration, $\langle r_G^2\rangle^{1/2}$) for each calculated molecular weight, the molecular structures of polymers in solution can be estimated. The slope from the plot of $\langle r_G^2\rangle^{1/2}$ *versus* M is useful for predicting the structure. The slope values are ~0.33 for spheres, 0.5–0.6 for random coils, and ~0.7 for random coils in a thermodynamically good solvent [28–30].

For monitoring light scattering, a DAWN-DSP MALS instrument ($\lambda = 632.8$ nm) and an Optilab DSP interferometric refractometer ($\lambda = 690$ nm) from Wyatt Technology (Santa Barbara, CA, USA) are utilized. The dn/dc of the polymer sample is also measured with the Optilab refractometer. To calculate the molecular weight and RMS radius values, a third-order polynomial fitting using the Berry method of the Debye plot is used with the MALS detector signals obtained from the detector angles 26, 35, 43, 52, 50, 69, and 80°.

3 Characterization of NaHA by FlFFF-MALS-DRI

3.1 Effect of field programming

The efficiency of field programming on the separation of NaHA using FI-AFlFFF channels can be demonstrated by comparing the elution profiles of a degraded NaHA sample extracted from *Streptococcus* (from LG Life Science, Daejon, Korea) using two different decay patterns, as shown in Fig. 2 [31]. The two fractograms shown in Fig. 2A are the light

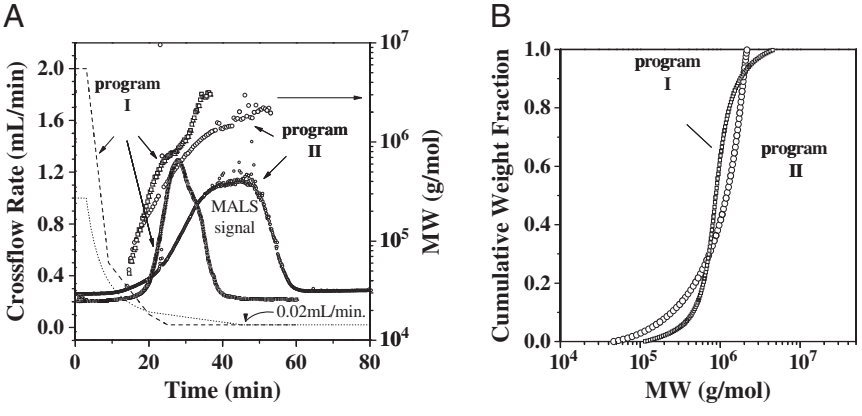

Figure 2. (A) Comparison of the LS signals obtained from two different flow rate conditions (programs I and II) along with the calculated molecular weights at each retention time slice and (B) the cumulative molecular weight distribution curves for NaHA at two different run conditions. Permission from [31].

scattering signals 90° from the MALS data obtained using two decay patterns (program I for linear decay and program II for power decay, see Eqs. 2 and 3). The initial crossflow rates, $\dot{V}_{c0}$, are 2.0 mL/min for program I and 1.0 mL/min for program II with an initial delay time fixed at 3 min for both runs, and the final crossflow rate, $\dot{V}_{cf}$, is fixed at 0.02 mL/min from 45 min for program I and from 25 min for program II. Incorporation of the fixed final cross flow rate is necessary to assure that sample components are not swept abruptly through the channel when the field strength becomes zero. The sample injection flow rates, $\dot{V}_s$, set to be identical to the outflow rate, $\dot{V}_{out}$, in the programming mode are 0.1 and 0.05 mL/min for programs I and II, respectively. Adjustment of the injection flow rate is based on the 1/20 rule in which the frit flow rate should be 20 times faster than the injection flow rate for efficient hydrodynamic relaxation. Fig. 2A shows the different elution fractograms along with the calculated MW values from the MALS measurements. Each data point in an MW value appears to increase as the retention time increases, showing that the separation of NaHA materials is accomplished in an increasing order of size; however, these increasing patterns differ due to differences in the decay patterns. Comparing the cumulative size distribution curves shown in Fig. 2B and the calculated average molecular weight values, MW, 1.04×10^6 for run I and 1.15×10^6 for run II, the results from both runs are similar. The dn/dc value for the sample used in Fig. 2 is measured as 0.165 mL/g. However, an advantage of using a higher initial frit flow rate and higher outflow rate conditions in program I yields a faster separation of the broad MW NaHA sample but with similar recovery values: $87.1 \pm 13.1\%$ ($n = 4$) for run I and $83.3 \pm 13.1\%$ ($n = 3$) for run II, based on comparison of the LS signal areas between runs obtained with and without field strength.

3.2 Effect of experimental run conditions

Owing to the complicated molecular interactions of water-soluble polymers in aqueous solution, a proper salt concentration is necessary to avoid extraordinary intermolecular and intramolecular electrostatic repulsions among NaHA molecules. In particular, intramolecular electrostatic repulsions influence the hydrodynamic sizes of NaHA molecules in solution. From a comparison of elution patterns of the same NaHA sample in Fig. 2 along with MW calculations at different ionic strengths (0.01, 0.05, and 0.1 M $NaNO_3$ solutions with 0.003 M NaN_3 added), retention of the NaHA sample with 0.1 M $NaNO_3$ solution has been shown to provide a satisfactory result, as shown in Fig. 2A, while the two more dilute solutions provide much faster elution but with poorer resolution in size fractionation, deduced from the inconsistency in the radii of gyration (data not shown). This effect can be explained by the NaHA molecules migrating further from the channel wall due to the influence of the increased electric double layer at lower ionic strengths [31].

The injection amount and volume of NaHA material introduced to the FI-AFlFFF channel need to be considered since too high of a concentration of sample material may induce unwanted aggregation. However, in FI-AFlFFF, samples are introduced at a relatively low flow rate (~0.1 mL/min), and injection of a large sample volume is not suggested due to the possible initial band broadening caused by a long injection time while the high-speed frit flow continuously enters the channel. When this is tested by varying the sample concentrations (0.8, 1.6, and 3.2 mg/mL) with a fixed injection volume (20 μL), consistency in retention time without overloading is observed for concentration levels up to 1.6 mg/mL (32 μg), as shown in Fig. 3 [31]. A higher injection amount causes a slight shift to a longer retention time, which may be caused by aggregation of NaHA molecules.

3.3 Effect of membrane filtration

When a membrane filtration process is applied to NaHA molecules, a significant change in size distribution is observed. To study the filtration effect on molecular weight distribution, an NaHA sample (dn/dc = 0.179, Shinpoong Pharmaceutical, Ansan, Korea) extracted from fowl sarcoma fluid was filtered through 0.2 and 0.45 μm pore size membranes [32, 33]. The FlFFF-MALS signals at 90° for the NaHA sample before and after filtration are shown in Fig. 4a (along with the calculated molecular weight value at each time slice.) The outflow rate is maintained at 0.1 mL/min throughout the runs. Apparently, the LS signal is reduced after filtration. However, the MW values of the three samples at each time slice are in good agreement, as

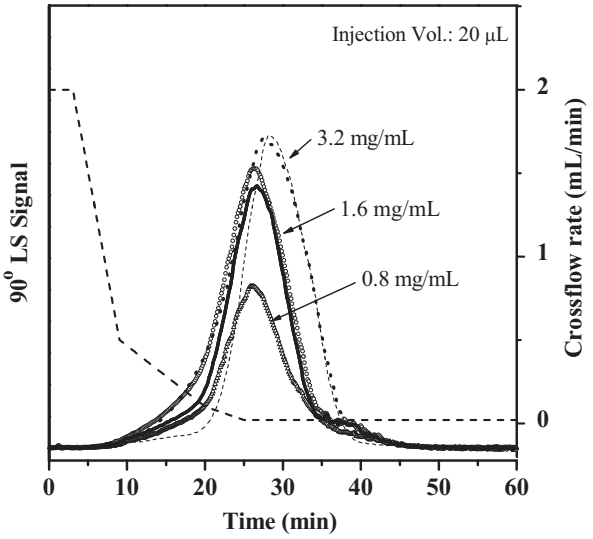

Figure 3. Influence of sample injection amount on retention of the NaHA sample by FI-AFlFFF represented with 90° LS signals. Signals of repeated measurements are overlayed. Injection volume was fixed at 20 μL with a variation of sample concentrations of 0.8, 1.6, and 3.2 mg/mL. The program I run condition from Fig. 2 was used at $I = 0.103$ M. Permission from [31].

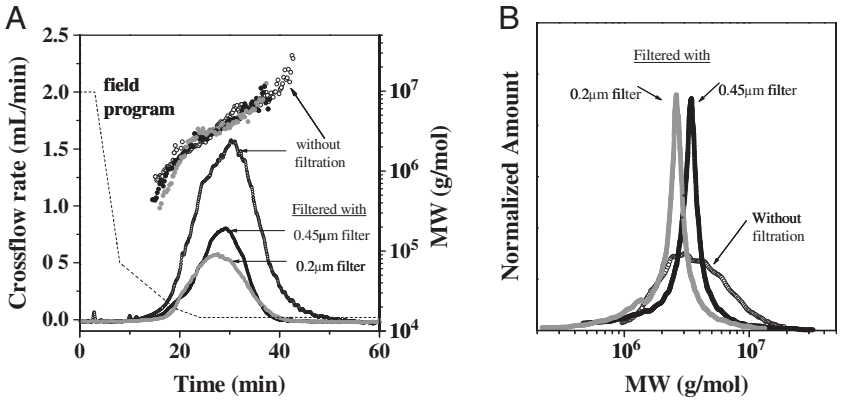

Figure 4. Effect of sample filtration on MWD of a raw NaHA sample dissolved at 5°C. Filtration was achieved using membrane filters with pore sizes of 0.2 and 0.45 μm. (A) Comparison of FI-AFlFFF fractograms (plotted with LS-90° signals) and calculated MW values along with field decay patterns. (B) Normalized MWD before and after filtration. Permission from [33].

seen in Fig. 4A. This result implies that there is a simple decrease in population due to filtration as is found in the clear difference in MWD curves shown in Fig. 4B. The calculated weight average molecular weight values decrease from $6.23 \pm 0.22 \times 10^6$ to $3.55 \pm 0.20 \times 10^6$ after filtration with the 0.45 μm pore membrane and to $3.10 \pm 0.19 \times 10^6$ with the 0.2 μm membrane ($n = 3$, each).

3.4 Effect of γ-radiation

γ-Radiation is often utilized to degrade polymers since it is known to be a reproducible method that induces a substantial change in the MWD due to hydrolysis. When raw NaHA material (different batch from sarcoma fluid, Shinpoong Pharmaceuticals, $dn/dc = 0.167$) is treated with γ-radiation of varying exposure periods, it exhibits significant size variation. Figure 5 shows the FlFFF fractograms (LS-90° signals and RI signals) of the control sample and three γ-radiation degraded samples indicated with 3 h (2.4 kGy), 8 h (5.3 kGy), and 10 h (7.4 kGy) periods of exposure [34]. The initial crossflow rate is maintained at $\dot{V}_{c0} = 2.0$ mL/min for 3 min and is decreased to 0.5 mL/min over 5 min, then to 0.1 mL/min over 7 min, then to 0.02 mL/min over 5 min, where it is maintained to the end of the run. A fractogram of the control sample (20 μg injection) shows a broad but smooth peak (open circles) between 20 and 50 min, and the calculated MW values plotted above the fractogram demonstrate that size fractionation in FlFFF is successfully achieved in the increasing order of size, up to 10^8 Da. With a radiation dose of 2.4 kGy, the radiated NaHA sample (marked as 2 h in Fig. 5) shows a significant shift to a shorter retention time, and the peak is narrower than that of the control sample; this shift becomes more evident with the 7.4 kGy sample. As the radiation dose increases, the concentration of NaHA molecules around 10 min increases significantly, as shown by the DRI signals. The MW values of the radiated samples calculated at each time slice show a consistent overlap except at the lower and upper MW limits. For the 2.4 kGy sample, a majority of the NaHA molecules is smaller than $\sim 3 \times 10^6$ g/mol, and the few data points above this MW limit are thought to be from erroneous calculation often found at the end of an elution as

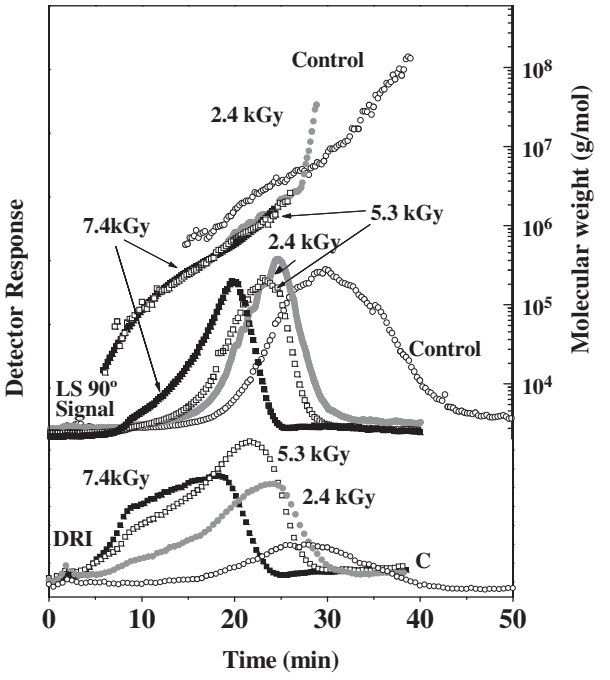

Figure 5. FlFFF fractograms (DRI signals at the bottom and MALS at 90°) of a raw NaHA sample superimposed with those of samples degraded by exposure to gamma radiation. MW values corresponding to each sample are plotted with different symbols but the same symbol convention is used. Samples marked with 2.4, 5.3, and 7.4 kGy represent doses of gamma radiation. Permission from [34].

the concentration decreases. For the 7.4 kGy sample, the lower limit of MW extends below 1×10^5 g/mol, and the upper limit decreases to $\sim 1 \times 10^6$ g/mol. The MWD curves of the four samples are compared in Fig. 6A, and the weight average and number average molecular weight values along with the average RMS radius values are listed in Table 1. The molecular weight values for the three degraded samples are less than those of the control sample, as shown in Fig. 5. The shift of the MW data points indicates that the retention time of species having identical molecular weights increases after exposure to gamma radiation, which can be explained by the conformation of degraded NaHA molecules having a more

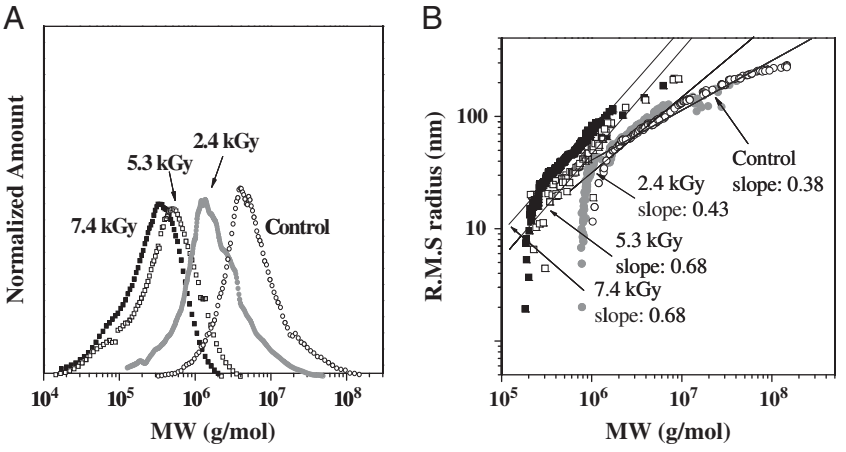

Figure 6. (A) Area normalized MWD curves of raw NaHA and the three degraded products shown in Figure 5 and (B) plots of RMS radius *versus* MW. Permission from [34].

Table 1. Effect of radiation dose, resulting in degradation, on Mw, RMS radius, and RSD values ($n = 4$) of NaHA samples. Radiation listed is the total amount. Permission from Ref. [34]

	Control sample	Degraded NaHA upon radiation doses		
		2 kGy	5 kGy	7 kGy
Mw (g/mol)	$(8.6 \pm 0.1) \times 10^6$	$(1.5 \pm 0.02) \times 10^6$	$(6.5 \pm 0.04) \times 10^5$	$(4.7 \pm 0.03) \times 10^5$
Mn (g/mol)	$(3.6 \pm 0.03) \times 10^6$	$(9.6 \pm 0.02) \times 10^5$	$(4.5 \pm 0.03) \times 10^5$	$(3.2 \pm 0.02) \times 10^5$
Mw/Mn	2.39 ± 0.04	1.19 ± 0.02	1.45 ± 0.02	1.32 ± 0.01
RMS radius (nm)	118.4 ± 0.5	62.0 ± 0.7	32.5 ± 1.2	31.8 ± 0.2

extended structure. This shape effect can be found in a typical FlFFF experiment since linear chain polymers have longer retention times due to the increase in hydrodynamic volume compared with that of a compact molecule of the same MW. This is supported by the comparison of slope values from the plots of RMS radius *versus* MW shown in Figure 6b. While the control sample has a slope of 0.38, representing a rather compact structure, the slope increases to 0.43 and 0.68 as the radiation dose is increased. This demonstrates that gamma radiation exposure effectively induces degradation of the NaHA molecules as well as an unfolding of the conformation to a more linear chain structure.

3.5 Effect of ultrasonic treatment

Ultrasonification generates small bubbles, produced by the rapid pressure change from the propagation of acoustic energy. The formation and collapse of bubbles induces a large velocity gradient around the bubbles, creating a mechanical force that can disrupt polymer chains, resulting in depolymerization [35]. When ultrasonication is applied to ultralarge MW NaHA molecules, the molecules are expected to degrade into smaller MW species or to experience loosening of the multiply folded helical NaHA chain structures. Figure 7 shows the fractograms of the control sample (another batch sample, $dn/dc = 0.142$) and two samples, LS-90° and DRI signals, sonicated for 4 and 8 h at 20 kHz, 20 W, at 4°C [36]. Because of the significant differences in the molecular weight ranges of the NaHA sample before and after sonication, two linear field decay patterns are employed (decay programs I and II in Fig. 7), and the outflow rate is fixed at 0.1 mL/min. For the control sample, decay program I is utilized for the FlFFF run, and the LS signals (black filled circles) appear as a unimodal distribution. The calculated MW data points of the control sample show a gradual increase in MW up to $\sim 10^8$ g/mol with an increase in retention time. Elution of the sonicated sample shows a significant shift in retention time (gray squares for 4 h, open circles for 8 h) with a subsequent decrease in the LS signals. However, the DRI signals increase significantly as the sonication time increases. This indicates that sonication induces a degradation or depolymerization of the NaHA molecules, resulting in an increase in detector responses from the population increase of smaller molecules since the LS signal depends on both concentration and MW, while DRI relies only on concentration. For the sonicated samples, a slightly modified decay pattern (program II) is utilized to provide a sufficient hydrodynamic relaxation for the smaller MW components by extending the initial delay time period. As shown from the MW data points above the fractograms (LS signals), the two degraded samples show critical differences in MW range compared with those of the control sample and to each other. The difference in MWD curves is shown in Fig. 8a, and the weight average and number average MW values

are listed in Table 2. From the calculated data, it is found that sonication for 8 h results in 25-fold decreases in MW and three-fold decreases in RMS radius; however, the polydispersity value is not significantly altered. From plots of RMS values against MW, as shown in Fig. 8B, sonication also creates structural changes in the NaHA molecules. The calculated slopes of the degraded sample increase to 0.62 and 0.75 for samples sonicated for 4 and 8 h, respectively, supporting a conformation change in the sonicated NaHA to a less entangled or linear structure from a compact, folded geometry.

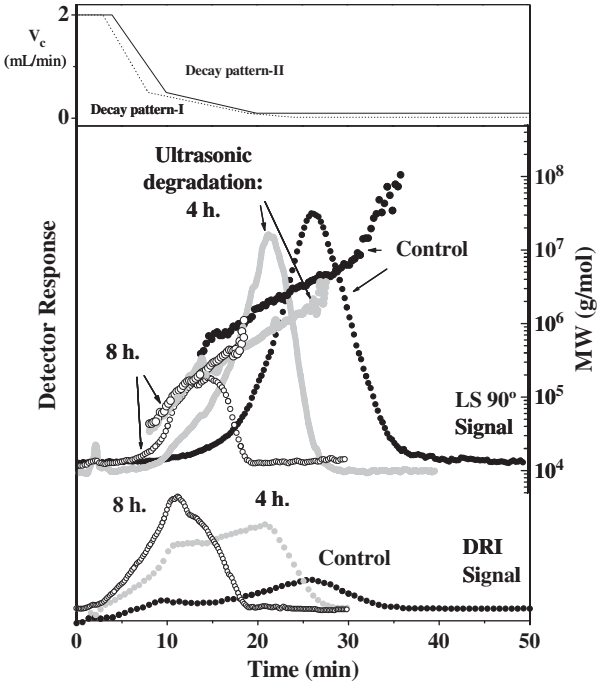

Figure 7. FIFFF fractograms (DRI signals at the bottom and MALS at 90°) of NaHA samples from ultrasonic degradation, and MW values calculated at each retention time slice. FIFFF separation of the control sample was carried out using field decay program-I, and the two degraded samples were run using decay program-II, both of which are provided at the top of the figure. Permission from [36].

3.6 Effect of enzymatic reaction

Enzymatic treatment of NaHA is a rather straightforward method for inducing chain scissions and is more rapid than the previously discussed methods. For instance, the same control sample used in Fig. 7 is treated with testicular hyaluronidase by varying the enzyme unit per mL of solution: 2 and 5 U/mL [36]. For each enzymatic reaction, the reaction time was selected to be either 0.5 or 1 h, resulting in four degraded samples labeled 2 U–0.5 h, 2 U–1 h, 5 U–0.5 h, and 5 U–1 h. Fractograms of the four degraded samples are plotted in Fig. 9 and are superimposed with DRI signals. For the control and the two 2 U samples, decay pattern I in Fig. 7 is utilized. However, for the two 5 U samples, decay pattern II is employed due to the significant reduction in the MW size after enzyme treatment. While the decreases in LS signal intensities and retention times for the samples treated with 2 Units of enzyme (2 U–0.5 h and 2 U–1 h) compared with that of the control are not significant, these parameters decrease dramatically for the two 5 U samples. On the other hand, the DRI signal intensity increases substantially due to the increase in concentration of smaller MW species after degradation. While treatment of the control sample with 2 U/mL of enzyme gives a relatively mild alteration in MWD, as shown in Fig. 10A, significant degradation can be obtained with 5 U/mL of enzyme in less than an hour. The weight average molecular weight values after enzymatic degradation with 2 U is already smaller than 1million g/mol seen in Table 2, indicating that a considerable amount of polymers larger than 10^6 g/mol are degraded. The weight average molecular weights for the samples treated with 5 U are less than $\sim 1 \times 10^5$ g/mol, and the polydispersity values are also decreased (1.43 and 1.39). Structural changes from the relationship of RMS radius *versus* MW can be estimated even for the 2 U enzyme treatment. From Fig. 10B, the

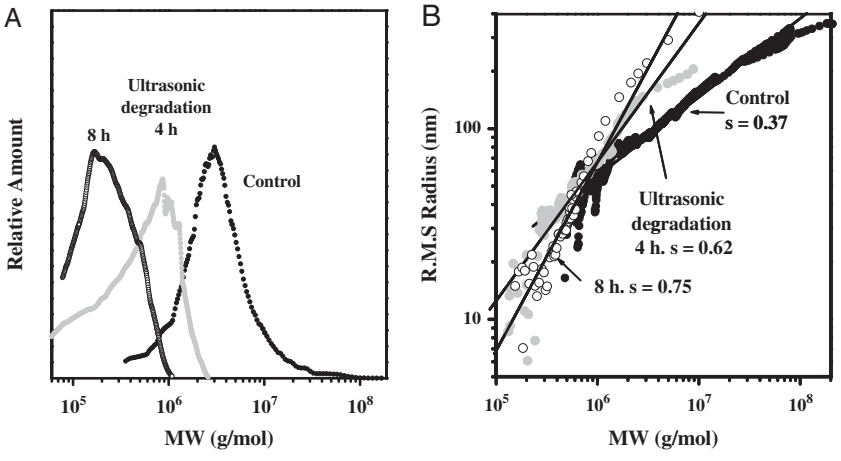

Figure 8. (A) Comparison of MWDs of NaHA before and after ultrasonic degradation and (B) plots of RMS radius *versus* MW values for the three NaHA samples. Permission from [36].

Table 2. Effect of degradation methods on Mw, Mn, RMS radius, and RSD values ($n = 4$) of the NaHA control sample. Permission from Ref. [36]

	Mw	Mn	Mw/Mn	RMS radius (nm)
Control sample	4.4 ($\pm$0.1) $\times 10^6$	2.2 ($\pm$0.02) $\times 10^6$	2.06 $\pm$ 0.04	107.6 $\pm$ 0.9
Ultrasonication				
4 h	5.3 ($\pm$0.04) $\times 10^5$	2.5 ($\pm$0.03) $\times 10^5$	2.03 $\pm$ 0.03	37.8 $\pm$ 0.3
8 h	1.7 ($\pm$0.1) $\times 10^5$	9.0 ($\pm$0.03) $\times 10^4$	1.91 $\pm$ 0.04	36.1 $\pm$ 0.5
Enzyme				
2 unit/0.5 h	8.2 ($\pm$0.05) $\times 10^5$	4.1 ($\pm$0.04) $\times 10^5$	2.03 $\pm$ 0.03	51.7 $\pm$ 0.1
2 unit/1 h	6.7 ($\pm$0.01) $\times 10^5$	3.3 ($\pm$0.03) $\times 10^5$	1.99 $\pm$ 0.02	49.7 $\pm$ 0.1
5 unit/0.5 h	9.0 ($\pm$0.2) $\times 10^4$	6.3 ($\pm$0.2) $\times 10^4$	1.43 $\pm$ 0.06	–
5 unit/1 h	8.2 ($\pm$0.1) $\times 10^4$	5.9 ($\pm$0.1) $\times 10^4$	1.39 $\pm$ 0.03	–

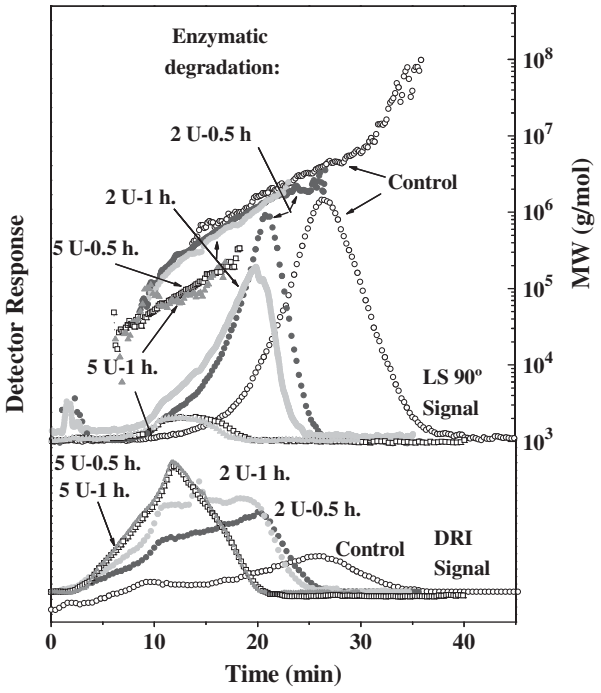

Figure 9. Effect of enzymatic degradations on the retention of NaHA materials by varying the number of enzyme units and the reaction period. Decay program-I was used for FlFFF separation of the degraded NaHA (2 U–0.5 h and −1 h), and program-II was used for the degraded samples (5 U–0.5 h and −1 h). Permission from [36].

slope values are 0.61 and 0.63 for the 2 U samples, denoting unfolding of entangled NaHA molecules. However, the RMS radius values for the samples treated with 5 U of enzyme are not clearly determined due to the large uncertainty in the calculation of smaller sizes.

3.7 Effect of thermal treatment

Another raw NaHA material from rooster comb and thermally treated samples are compared by elution pattern and molecular weight distribution using FlFFF-MALS-DRI. Thermal treatment is performed by heating the raw material (10 mg/mL in 0.3 M NaCl solution) at 100°C for 5–30 min in 5 min intervals, and the resulting solutions are diluted with 0.1 M $NaNO_3$ to 0.8–1.0 mg/mL and left overnight without stirring at 4°C. Figure 11A shows the fractograms of the four samples (control and samples treated thermally for 10, 20, and 30 min) including both the LS and DRI signals [37]. In the figure, F3 and F4 (marked with slashes) are the time intervals for two collected fractions that will be explained later. The calculated molecular weight values of the control sample (marked as open triangles in both the fractogram and MW) show a gradual increase in MW upon an increase in retention time, as well as a broad MW distribution (10^6–10^8 g/mol). Fractograms of the thermally treated samples show reduced signal intensities, as is observed in the other degradation processes. However, increased patterns of calculated MW points between 20 and 30 min are similar among the four samples, in which smaller molecules may have similar structures regardless of the thermal treatment time. However, for the samples having undergone thermal treatment, the calculated MW points after 30 min are clearly different from those of the control sample. This can be explained by shape differences resulting in a shift in the FlFFF retention: linear molecules are retained longer than are spherical molecules with the same MW. Even after 10 or 20 min of thermal treatment, the ultrahigh MW portion ($> 2 \times 10^7$ Da) of the sample is no longer observed while the population of the smaller MW portion ($< 10^6$ Da) does not increase. This is easily recognized by superimposing the cumulative MWDs of the four samples as shown in Fig. 11B. First, because the ultrahigh MW molecules are not observed during the early thermal treatment (10 or 20 min) or after 30 min of treatment, the population of lower MW species appears to increase. From this experiment, structures of the ultrahigh MW ($> 2 \times 10^7$ Da) regime can be estimated to some degree as will be explained later. Calculated MW and RMS radius values are listed in Table 3 along with the slope values for the RMS radius-MW plot. As the thermal treatment period increases, the slope values increase from 0.33 (10 min) to 0.43 (20 min) to 0.59 (30 min), indicating a trend to extended structures. Thus, thermal treatment is a relatively

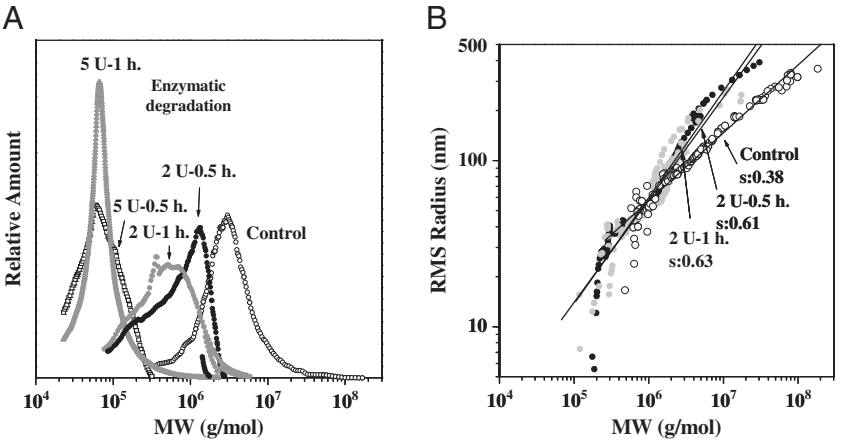

Figure 10. (A) Influence of enzymatic degradation on MWDs of NaHA samples corresponding to the fractograms shown in Figure 9, and (B) plots of RMS radius *versus* MW values for the enzymatically degraded NaHA products. Permission from [36].

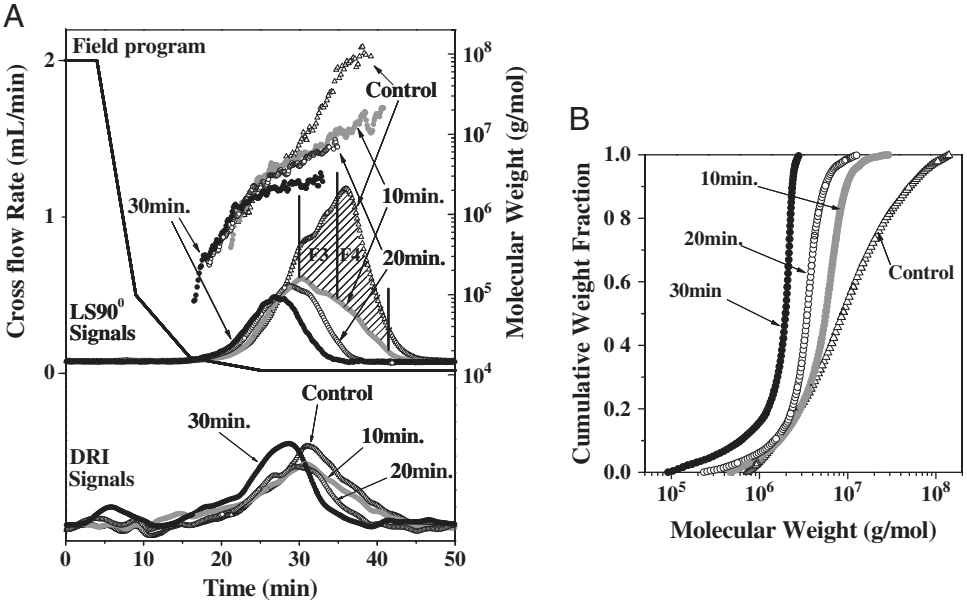

Figure 11. (A) FlFFF fractograms (DRI signals at the bottom and MALS at 90°) of NaHA samples (control sample and three thermally treated samples), and MW values calculated at each retention time slice. Fractions F3 and F4 were collected during the separation of the control sample for the separate thermal treatments. (B) Cumulative molecular weight distributions of the control NaHA sample before and after thermal treatment. Permission from [37].

Table 3. Calculated Mw, Mn, RMS radius, and slope values of the thermally treated NaHA samples compared with those of the control sample. Permission from Ref. [37]

	Mw (g/mol)	Mn (g/mol)	Mw/Mn	RMS radius (nm)		Slope
				Rw	Rn	
Control	$(1.92 \pm 0.04) \times 10^7$	$(4.89 \pm 0.07) \times 10^6$	3.92 ± 0.10	142.3 ± 0.6	104.3 ± 0.4	0.30
5 min	$(7.91 \pm 0.11) \times 10^6$	$(4.26 \pm 0.05) \times 10^6$	1.86 ± 0.03	119.7 ± 0.5	104.5 ± 0.4	0.31
10 min	$(5.77 \pm 0.07) \times 10^6$	$(3.40 \pm 0.04) \times 10^6$	1.68 ± 0.03	111.9 ± 0.5	96.8 ± 0.5	0.33
15 min	$(4.40 \pm 0.04) \times 10^6$	$(3.97 \pm 0.04) \times 10^6$	1.11 ± 0.01	97.0 ± 0.3	92.9 ± 0.3	0.39
20 min	$(3.90 \pm 0.03) \times 10^6$	$(3.27 \pm 0.02) \times 10^6$	1.19 ± 0.01	95.2 ± 0.3	77.5 ± 0.4	0.43
25 min	$(2.76 \pm 0.02) \times 10^6$	$(1.59 \pm 0.02) \times 10^6$	1.73 ± 0.02	94.9 ± 0.4	76.0 ± 0.5	0.45
30 min	$(1.76 \pm 0.01) \times 10^6$	$(1.59 \pm 0.01) \times 10^6$	1.65 ± 0.02	87.0 ± 0.3	68.0 ± 0.4	0.59

mild degradation process compared to the previously described methods in this review.

It is interesting to examine whether the ultrahigh MW fraction of the raw material during thermal treatment is first broken into smaller fragments or is disaggregated. In order to elucidate the mechanism, two fractions of the ultrahigh MW regime during the FlFFF elution of the control sample are collected at time intervals marked in Fig. 11 as slanted

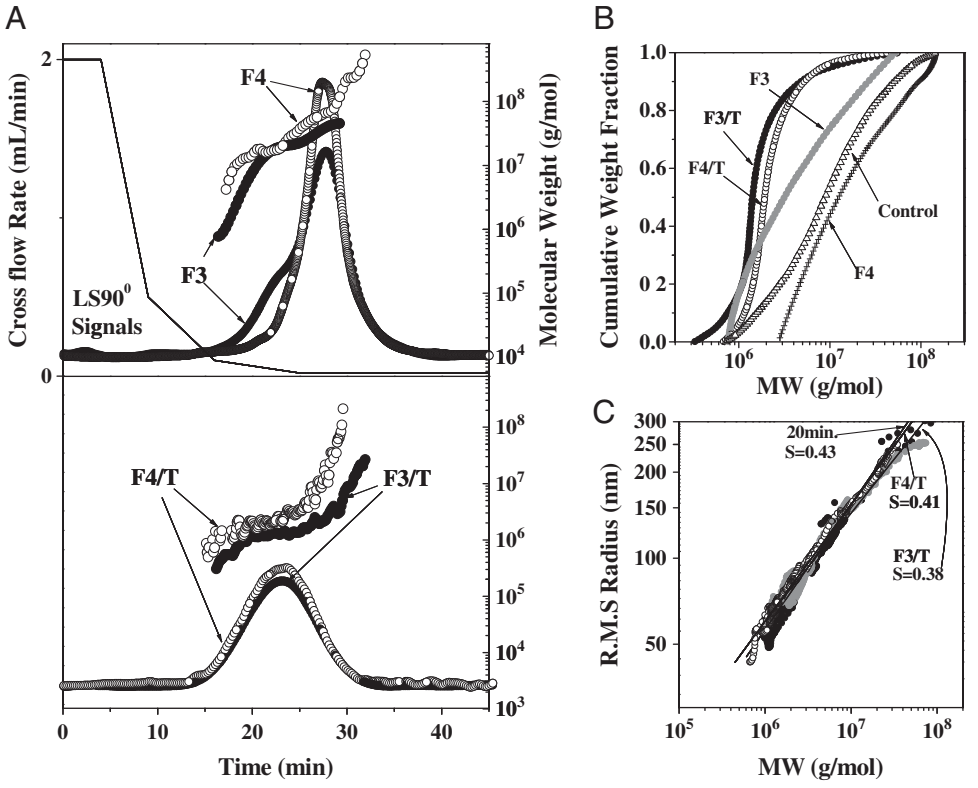

Figure 12. (A) Comparison of LS signals of re-injected FlFFF fractions before (F3 and F4 marked in Fig. 11) and after thermal treatment (F3/T and F4/T), (B) the superimposed cumulative distribution curves of the two fractions with the control sample, and (C) plots of RMS radius *versus* MW values of the thermally treated fractions, F3/T and F4/T. Permission from [37].

lines: F3, 30–35 min, and F4, 35–40 min. Fractions F3 and F4 (accumulated 20 times each) are treated using the same method (100°C for 20 min), and the resulting fractions, labeled F3/T and F4/T, respectively, and all fractions are re-injected into the FlFFF-MALS-DRI. Figure 12A shows the FlFFF fractograms of F3 and F4 before the thermal treatment (at the top) and of F3/T and F4/T after thermal treatment. The LS signals of the F3 and F4 fractions appear to be similar; however, the smaller-MW regions ($<10^7$ Da) differ when comparing the MWD curves from Fig. 12a (top) and Fig. 12B. After thermal treatment, fractograms of F3/T and F4/T (bottom of Fig. 12A) appear to be similar, with a slight difference in calculated MW values, and they are shifted to shorter retention times with a broader MW distribution. Examination of the cumulative distribution curves of these fractions, F3/T and F4/T, in Fig. 12B shows that the relative amount of the larger-MW portion ($>10^7$ Da) of both fractions is less than 10% by weight. Moreover, the smaller-MW portion ($<10^6$ Da) of fraction F3/T does not substantially increase. From these observations, it appears that chain degradation from the ultrahigh MW portion of the F3 fraction (20 min of treatment) is not likely a contributing factor in the reduction of the size distribution because the smaller-MW species ($<10^6$ Da) does not significantly increase as the ultrahigh MW molecule population decreases. Instead, looking at the cumulative weight distributions of F3/T and F4/T in comparison with those of F3 and F4 (see Fig. 12B), the intermediate MW regime population (10^6~10^7 Da) is found to greatly increase. The slopes from the plots of RMS radius *versus* MW for F3/T and F4/T are 0.38 and 0.41, respectively, as shown in Fig. 12C, similar to the value of the control sample treated for 20 min (slope = 0.43). From these observations, it can be deduced that the ultrahigh MW portion ($>10^7$ Da) of the raw NaHA sample originates from supermolecular structures formed by aggregation of intermediate sized molecules (10^6–10^7 Da). These data support the multi-fold helical structures that were suggested in an earlier work [11].

4 Concluding remarks

This review summarizes a series of studies on ultrahigh MW sodium hyaluronate materials using FlFFF-MALS-DRI for size characterization as well as structural variations depending on the purification and refining processes utilized in the intermediate stage of development for pharmaceutical applications. Since NaHA materials can have a very broad MWD with an exceptionally high MW limit, FlFFF provides a unique capability to successfully fractionate these molecules without fear of sample interactions with packing materials, an occurrence often observed in chromatographic methods. In addition, sample materials can be injected without the filtration, which has been known to cause a serious loss or alterations to the original characteristics of such large MW species. To achieve the full benefit of the FlFFF capability, proper field-programming parameters such as initial field strength and decay pattern are optimized according to the size distribution of

NaHA species. Moreover, the ionic strength of the carrier solution, injection amount, and sample concentration are critical in the analysis of water-soluble polymers using FlFFF. From the various depolymerization processes for NaHA described in this study, it is shown that enzymatic degradation is the most powerful method in terms of time-dependent degradation efficiency as well as conformational change to unfolded and extended structures, although each of the degradation methods has merits of speed of degradation and gentle or mild reduction of size distribution without significant structural changes. The combination of FlFFF, MALS and DRI has been demonstrated to be capable of monitoring structural changes and MWD in the study of polymer chemistry as well as in the development of applications.

This study was supported by a National Research Foundation Grant (NRF-2010-0014046).

The authors have declared no conflict of interest.

5 References

[1] Iqbal, Z., Midgley, J. M., Watson, D. G., Karditsas, S. D., Dutton, G. N., Wilson, W., *Pharm. World Sci.* 1997, *19*, 246–250.

[2] Yeung, B., Marecak, D., *J. Chromatogr. A* 1999, *852*, 573–581.

[3] Vercruysse, K. P., Prestwich, G. D., *Crit. Rev. Ther. Drug Carrier Syst.* 1998, *15*, 513–555.

[4] Motohash, N., Nakamichi, Y., Mori, I., Nishijawa, H., Umemoto, J., *J. Chromatogr.* 1988, *435*, 335–342.

[5] Sasari, H., Konttinen, T. Y., Santavirta , S., *Med. Sci. Res.* 1989, *18*, 99–101.

[6] Takahashi, R., Al-Assaf, S., Williams, P. A., Kubota, K., Okamoto, A., Nishinari, K., *Biomacromolecules*, 2003, *4*, 404–409.

[7] Mengher, L. S., Pandher, K. S., Bron, A. J., Davey, C. C., *Br. J. Opthalmol.* 1986, *70*, 442–447.

[8] Miyazaki, S., Yomota, C., Okada, S., *J. Ocul. Pharmacol.* 1996, *12*, 27–34.

[9] Rehakova, M., Bakos, D., Soldan, M., Vizarova, K., *Int. J. Biol. Macromol.* 1994, *16*, 121–124.

[10] Yang, B. Y., Montgomery, R., *Bioresour. Tech.* 2007, *98*, 3084–3089.

[11] Livant, P., Roden, L., Krishna, R., *Carbohydr. Res.* 1992, *237*, 271–281.

[12] Motohashi, N., Mori, I., *J. Chromatogr.* 1984, *299*, 508–512.

[13] Shimada, E., Nakamura, K. T., *J. Chromatogr. A.* 1994, *685*, 172–177.

[14] Kvam, C., Granese, D., Flaibani, A., Zanetti, F., Paoletti, S., *Anal. Biochem.* 1993, *211*, 44–49.

[15] Giddings, J. C., *Anal. Chem.* 1981, *53*, 1170A–1178A.

[16] Giddings, J. C., *Science* 1993, *260*, 1456–1465.

[17] Wahlund, K.-G., Giddings, J. C., *Anal. Chem.* 1987, *59*, 1332–1339.

[18] Ratanathanawongs, S. K., Giddings, J. C., *Anal. Chem.* 1992, *64*, 6–15.

[19] Moon, M. H., Kang, D., Hwang, I., Williams, P. S., *J. Chromatogr. A* 2002, *955*, 263–272.

[20] Reschiglian, P., Moon, M. H., *J. Proteomics* 2008, *73*, 265–274.

[21] Thielking, H., Roessner, D., Kulicke, W.-M., *Anal. Chem.* 1995, *67*, 3229–3233.

[22] Wittgren, B., Wahlund, K.-G., *J. Chromatogr. A* 1997, *760*, 205–218.

[23] Fraunhofer, W., Winter, G., Coester, C., *Anal. Chem.* 2004, *76*, 1909–1920.

[24] Picton, L., Bataille, I., Muller, G., *Carbohydrate Polymers* 2000, *42*, 23–31.

[25] Moon, M. H., Kwon, H. S., Park, I., *Anal. Chem.* 1997, *69*, 1436–1440.

[26] Moon, M. H., Williams, P. S., Kwon, H., *Anal. Chem.* 1999, *71*, 2657–2666.

[27] Kang, D. J., Moon, M. H., *Anal. Chem.* 2004, *76*, 3851–3855.

[28] Wyatt, P. J., *Anal. Chim. Acta* 1993, *272*, 1–40.

[29] Wittgren, B., Wahlund, K.-G., *J. Chromatogr. A* 1997, *791*, 135–149.

[30] Andersson, M., Wittgren, B., Wahlund, K.-G., *Anal. Chem.* 2003, *75*, 4279–4291.

[31] Lee, H., Kim, H., Moon, M. H., *J. Chromatogr. A* 2005, *1089*, 203–210.

[32] Kim, H., Lee, H., Moon, M.H., *Bull. Korean Chem. Soc.* 2006, *27*, 413–418.

[33] Lee, H., Cho, I.-H., Moon, M. H., *J. Chromatogr. A* 2006, *1131*, 185–191.

[34] Shin, D. Y., Hwang, E. J., Cho, I.-H., Moon, M. H., *J. Chromatogr. A* 2007, *1160*, 270–275.

[35] Basedow, A. M., Ebert, K., *Adv. Polym. Sci.* 1977, *22*, 83–148.

[36] Moon, M. H., Shin, D. Y., Lee, N., Hwang, E., Cho, I.-H., *J. Chromatogr. B* 2008, *864*, 15–21.

[37] Kwon, J. H., Hwang, E., Cho, I.-H., Moon, M. H., *Anal. Bioanal. Chem.* 2009, *395*, 519–525.

